Internal Transport Barrier with Ion-Cyclotron-Resonance Minority Heating on Tore Supra

G. T. Hoang, C. Bourdelle, X. Garbet, G. Antar, R. V. Budny,* T. Aniel, V. Basiuk, A. Bécoulet, P. Devynck, J. Lasalle, G. Martin, F. Saint-Laurent, and the Tore Supra Team

Département de Recherches sur la Fusion Contrôlée, Association Euratom-CEA, CEA Cadarache, 13108 Saint-Paul-lez-Durance, France

(Received 15 February 2000)

Recently, reversed magnetic shear operation was performed using only ion-cyclotron-resonance frequency minority heating (ICRH) during current ramp-up. A wide region of reversed magnetic shear has been obtained. For the first time, an electron internal transport barrier sustained by ICRH is observed, with a dramatical drop of density fluctuations. This barrier was maintained, on the current flat top, for about 2 s.

PACS numbers: 52.55.Fa, 52.25.Fi, 52.25.Gj, 52.50.Gj

Reversed magnetic shear (RS) plasma configuration with internal transport barrier (ITB) is one of the most promising ways to achieve high performance regimes, as proved in many tokamaks: TFTR [1], DIII-D [2], JT-60U [3], and JET [4]. It has been observed for the first time in JET experiments [5], in which the ion-cyclotron-resonance frequency minority heating (ICRH) power was applied during the current rise combining with pellet injection (PEP mode). Tore Supra (major radius $R \leq 2.4$ m, minor radius $a \leq 0.8$ m, toroidal magnetic field $B_T \leq 4.2$ T, and plasma current $I_p \leq 2$ MA), has also demonstrated the sustainment of RS plasma with noninductive current drive by lower hybrid waves [6]. Steady-state RS plasmas were maintained for up to 2 min [7]. A narrow electron ITB, within normalized radius r/a of 0.3, was obtained at relatively low plasma density (central density $n_e(0) \leq 3 \times 10^{19}$ m^{-3}) and low I_p ($\leq$0.8 MA). The attractive method used in [1–4] consists in applying neutral beam heating very early in the discharge during the plasma current ramp-up. However, in Tore Supra, this method cannot be easily used with ICRH because the density is usually too low, during the start-up phase, to obtain a good power coupling. For Tore Supra circular plasmas, the time required for reaching a density high enough to couple the ICRH power, by gas puffing, is much larger than the resistive time scale (a few hundreds of ms).

This paper reports a scenario recently investigated in Tore Supra for high-density and high-plasma current operation, using only ICRH minority scheme for ITB formation. For the first time, an evident electron ITB at moderate ICRH power ($P_{\rm rf} < 4$ MW), accompanied by a reduction of density fluctuations, leads to an increase of global energy confinement of about 50%.

The technique used consists in preforming a hollow current density profile (j) by minimizing the edge resistive skin depth during the rapid I_p ramp-up, i.e., efficient freezing of the resistive current diffusion. The skin depth is defined as $\delta \approx (2\eta/\omega_{\rm ramp})^{0.5}$. η and $\omega_{\rm ramp}$ are, respectively, the plasma resistivity and the current ramp-up rate [$\omega_{\rm ramp} \approx (1/I_p)(dI_p/dt)$]. To minimize δ one should increase $\omega_{\rm ramp}$ and/or reduce η (by electron heating localized at the edge, for example, using electron cyclotron resonance heating). In our experiments, the ICRH heating is not necessary for the formation of the hollow current profile as in the previously mentioned experiments. The ICRH power is applied after the formation of the RS configuration by optimization of $\omega_{\rm ramp}$ during the ramp-up. The scenario consists in setting a low I_p flat top phase ($\leq$0.4 MA) long enough (several seconds) to reach a steady state (Fig. 1). The plasma current is then rapidly ramped up to 1.2 MA. The first stationary flat top phase is required for (i) high-density operation, up to 7×10^{19} m^{-3} (about 0.65$\times$ Greenwald limit [8]) by gas fueling; (ii) a stationary and large enough pressure profile to avoid the onset of magnetohydrodynamics activity during the rapid current ramp-up at the rate $dI/dt = 1.6$ MA/s. Another advantage of such a scenario

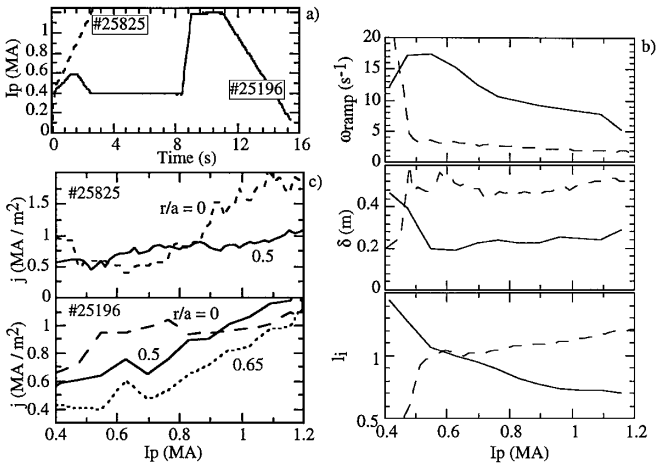

FIG. 1. Comparison between two scenarios, with and without low stationary I_p: (a) Plasma current. (b) Ramp-up rate, skin depth (at $r/a = 0.7$), and self-inductance versus total current for two scenarios. Case 1 (full curve): ramp-up between 8.5 and 9 s, after a steady state $I_p = 0.4$ MA. Case 2 (dashed curve): start-up phase between 0.1 and 2.5 s. (c) Evolution of current density at various radii during the plasma current ramp-up from 0.4 to 1.2 MA for shots in (a).

is to obtain a stationary density high enough for coupling a large amount of ICRH power.

In Fig. 1(b), the evolutions of ω_{ramp}, δ, and self-inductance (l_i) when I_p is ramped up from 0.4 to 1.2 MA, before ICRH power application, are shown for two scenarios: discharges No. 25196 and No. 25825 [Fig. 1(a)]. Both discharges have been carried out at the central density of 6.5×10^{19} m^{-3}, and the working gas is helium. For shot No. 25196, I_p is raised at the rate $dI_p/dt = 1.6$ MA/s, after a 0.4 MA stationary phase of several seconds. It differs from shot No. 25825 where I_p is ramped in the early time of the discharge at $dI_p/dt = 0.35$ MA/s. During the current ramp-up of shot No. 25196, ω_{ramp} is maintained at a high value of about 10 s^{-1}, which induces a thin skin depth at the edge (normalized radius $r/a = 0.7$) of about 0.2 m ($a = 0.75$ m) compared to the value of 0.5 m in shot No. 25825. As a consequence, a drop of l_i to a low value around 0.7 is observed, characterizing a broadening of the current profile. Conversely, l_i increases to the value of 1.2 in shot No. 25825, which indicates a peaked profile. In Fig. 1(c), the evolution of the current density is plotted at various radii. Here the current density profiles are obtained from the Faraday rotation angles (α_F) measured by a five chords infrared polarimetry, with a time resolution of 1 ms and a spatial resolution of 2 cm. Absolute error on the measurement of α_F is $\pm 0.25 \times 10^{-2}$ rad, corresponding to a systematic error in the range of 5% at the midradius and 25% in the center. It can be seen that the central current density is effectively frozen in shot No. 25196 when I_p increases from 0.6 to 1.2 MA. The added resistive current (0.6 MA) is mostly accumulated in the edge region $0.5 < r/a < 1$ [Fig. 2(b)]. The value at midradius increases from 0.5 to 1.2 MA/m^2 and becomes higher than the central value which is almost constant (less than 1 MA/m^2). For shot No. 25825, the opposite behavior of the current diffusion is observed. The resistive current rapidly diffuses to the core region: the central value rises from 0.6 to 1.8 MA/m^2, exceeding the midradius value which weakly increases.

Once the hollow j profile is preformed, ICRH is applied for ITB formation. An ICRH power up to 4 MW is applied at the end of the I_p ramp-up. The time evolution of the current density profile during the 4 MW pulse of ICRH is shown in Fig. 2(b). The RS configuration is preformed during the current ramp-up (at $t = 8.7$ s), with central value of safety factor, $q(0)$, between 2.5 and 3. It is transiently maintained on the 1.2 MA flat top for about 0.2 s, from $t = 9$ s to $t = 9.2$ s, when ICRH is applied. Within the error bars the minimum value of q (about 2) is found to be located between $r/a = 0.5$ and $r/a = 0.6$ [Fig. 2(c)]. This transient hollow profile relaxes to a flat profile. In spite of a dominant on-axis electron heating the flat profile remains until the end of the I_p plateau ($t = 11$ s). With ICRH an electron internal barrier is observed at $r/a = 0.6$. From the time traces of electron

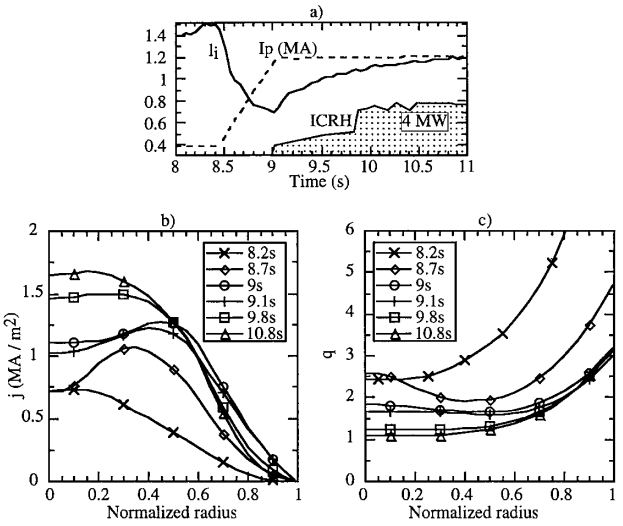

FIG. 2. ICRH H-minority heating discharge with preformed hollow current profile (No. TS25196): (a) Plasma current, self-inductance, and ICRH power. (b) Evolution of current density profile, before (at $t = 8.2$ s and $t = 8.7$ s) and during ICRH application (at $t = 9$, 9.1, 9.8, and 10.8 s). (c) Corresponding safety factor (q) profiles.

temperature and density, shown in Figs. 3(a) and 3(b), this barrier seems to be formed at around $t = 9.2$ s. Both the temperature and density increase inside the region $r/a = 0.6$, while the total power is kept constant and the power deposition profile is unchanged [Fig. 4(b)]. The gas fueling is also switched off at $t = 9$ s. The electron pressure gradient, shown in Fig. 4(a), significantly increases within $r/a < 0.6$ where the magnetic shear is lower than that in the reference L-mode discharge (0.3 instead of 0.7 in the L mode). Note that the ITB is observed with a moderate ICRH power. Indeed, as indicated in Fig. 4(a) the pressure obtained with $P_{\text{rf}} = 2$ MW (2.7 MW of total power) is quite the same as the L mode one performed with 4 MW (4.5 MW of total power). The electron energy exceeds the Rebut-Lallia-Watkins L-mode scaling [9] by a factor of 1.4 [Fig. 3(c)]. Also, the global energy confinement time is found higher than the ITER L-mode prediction [10] [Fig. 3(d)]. The enhancement factor H is about 1.4 (confinement time $\tau_E = 130$ ms compared to 95 ms of a reference L-mode shot, and $\tau_E^{\text{ITER-}L} = 90$ ms). Both scaling fairly well reproduce the L-mode Tore Supra discharges [11]. No information on ion channel was available, but the same enhancement factor in both total and electron energies suggests that the ion confinement may also be improved.

One-fluid transport analysis shows that the effective heat diffusivity (χ_{eff}) is significantly reduced from the L-mode value in the flat q-profile region. Figure 4(b) shows the profile of χ_{eff} of shot No. TS25196 for three time slices during the improved confinement phase: 0.3, 0.7, and 1 s after the ITB formation ($t = 10.1$, 10.5, and 10.8 s) together with a reference L-mode shot. For this analysis, the

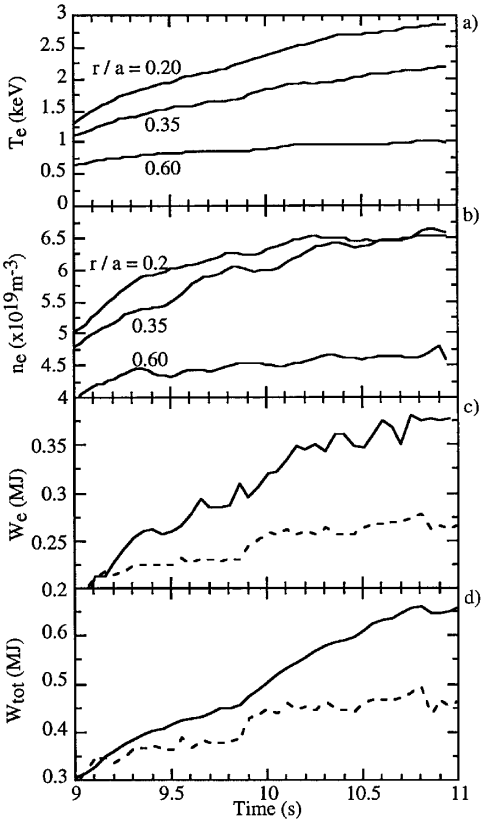

FIG. 3. Time evolution, during ICRH, of shot No. TS25196 shown in Fig. 2: (a) Electron temperature at different normalized radii ($r/a = 0.2$, 0.35, and 0.6). (b) Electron density at different normalized radii ($r/a = 0.2$, 0.35, and 0.6). (c) Electron energy (full curve) and the electron Rebut-Lallia-Watkins L-mode scaling (dashed curve). (d) Total energy (full curve) and the ITER L-mode scaling (dashed curve).

ICRH power deposition is computed by the PION code [12]. The calculation gives a power coupled to the electrons of about 80% of 4 MW injected power with an unchanged deposition profile during the improvement phase.

For this experiment, the density fluctuations are measured by heterodyne CO_2 laser scattering diagnostic for $k = 8\ \mathrm{cm}^{-1}$. The results indicate that the turbulence intensity, during the current ramp-up phase when the hollow current profile is formed, is significantly reduced and remains at a low level during the ICRH power application. Time trace of normalized rms $[(dn/n)^2]$ is compared to the level of a corresponding L-mode shot in Fig. 5(a). The burst that occurred at $t = 8.5$ s is due to a fast change of plasma position at the beginning of the ramp-up. The reduction of the signal is observed at $t = 8.7$ s where the hollow q profile is formed. A statistic analysis of a series of shots is shown in Fig. 5(b). This figure shows that the normalized rms signal decreases with increasing $n_e \nabla T_e$, while an opposite variation is usually observed in the L mode [13]. The frequency spectra of the turbulence are shifted by the Doppler effect associated with the $\mathbf{E} \times \mathbf{B}$ flow. The time evolution of this shift allows us to conclude that an increase of the $\mathbf{E} \times \mathbf{B}$ shear takes place during the stabilization of the turbulence level. Since the turbulence is measured at $k = 8\ \mathrm{cm}^{-1}$ and the value of $k\rho_i$ (ρ_i being ion Larmor radius) in the measurement region is about 0.3, both components of the turbulence (electronic and ionic) are represented in the frequency spectrum. Therefore, the reduction of the fluctuation level could be affected by both of them. Detailed analysis of the behavior of turbulence during this experiment is done in Ref. [14].

A stability analysis has been performed with a gyrofluid code [15]. This code consists in solving the gyrofluid equations using the ballooning representation at lowest order and Gaussian trial functions. This technique allows calculating the growth rates of microinstabilities over a wide range of toroidal wave numbers and magnetic surfaces. In this limit, stabilizing effects of weak or negative magnetic shear are expected: (i) negative value of s stabilizes the interchange drive, (ii) vanishing of absolute value of s to zero increases the distance between resonance surfaces

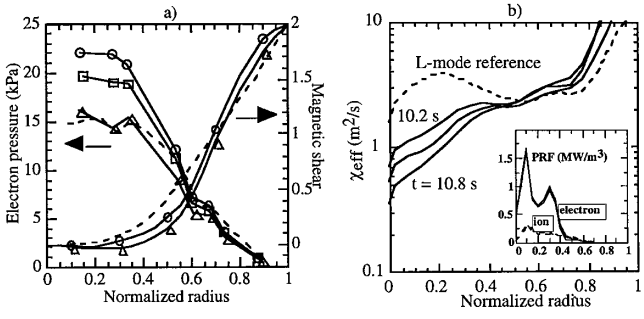

FIG. 4. Radial profiles for shot No. TS25196 in Fig. 2: (a) Electron pressure and magnetic shear, at $t = 9.8$ s (triangles, 2 MW), $t = 10.2$ s (squares, 4 MW), and $t = 10.8$ s (circles, 4 MW). Dashed curve corresponds to the reference L-mode shot performed with 4 MW of ICRH power. (b) One-fluid effective electron heat diffusivity, at $t = 10.2$, 10.5, and 10.8 s, compared with the L-mode reference one.

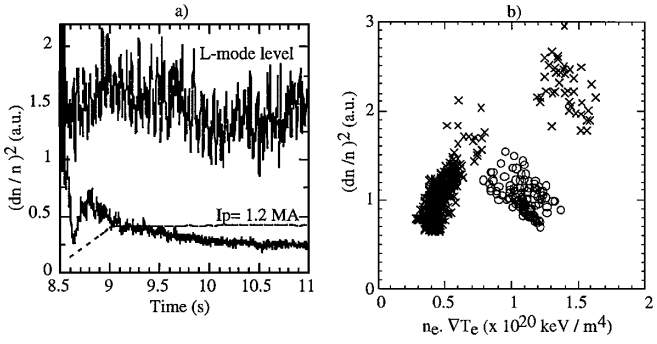

FIG. 5. Density fluctuations from CO_2 laser scattering diagnostic for $k = 8\ \mathrm{cm}^{-1}$: (a) Normalized rms $[(dn/n)^2]$ of a shot of scenario described in this paper (No. TS25186) and of its reference L-mode shot (No. TS26580), performed at the same plasma parameters, $I_p = 1.2$ MA. (b) Variation of density fluctuations with $n_e \nabla T_e$ (crosses, ICRH L-mode shots; circles, ICRH shots with preformed hollow q-profile).

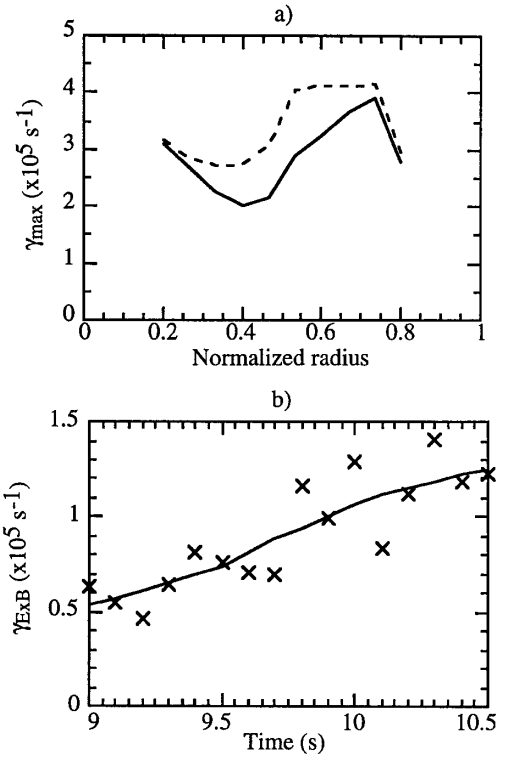

FIG. 6. Stability analysis of shot No. TS25196: (a) Radial profile of maximum growth rate calculated at $t = 9.1$ s for measured hollow q-profile (full curve) and for an assumed monotonic q-profile (dashed curve). (b) Time evolution of shearing rate during ICRH application.

and stabilizes the slab branch for passing particles. Those growth rates are overestimated compared to kinetic calculations and they do not account for the stabilizing effect of $\mathbf{E} \times \mathbf{B}$ shear. The later effect is investigated by comparing the maximum growth rate ($\gamma_{\max}$) on each magnetic surface with the shearing rate [$\gamma_{\mathbf{E}\times\mathbf{B}} = (1/B)\,(dE_r/dr)$]. Because of the rather high level of ripple, the radial electric field on Tore Supra can be determined by the ambipolarity condition on ripple thermal particle losses [16,17].

The radial profile of $\gamma^{\max}$ at $t = 9.1$ s, where the q profile is hollow, is compared with the computed value of $\gamma_{\max}$ assuming a monotonic q profile in Fig. 6(a). One can see that the negative value of s reduces $\gamma_{\max}$ in the core region. In the plateau, this effect diminishes because the current density relaxes to the monotonic profile. $\gamma_{\max}$ increases due to the increase of the pressure gradient. However, at the same time, a larger $\gamma_{\mathbf{E}\times\mathbf{B}}$ induced by more peaked density and temperature profiles could take place for stabilization [18]. As shown in Fig. 6(b), $\gamma_{\mathbf{E}\times\mathbf{B}}$ increases by a factor of about 2 between $t = 9.1$ s and $t = 10.5$ s.

In summary, we have demonstrated that the electron ITB can be sustained by application of the ICRH on the nonmonotonic q-profile target by optimizing of the current ramp-up. The uncertainties on $\gamma_{\mathbf{E}\times\mathbf{B}}$ as well as on the overestimated value of $\gamma_{\max}$ do not allow firm conclusions. Nevertheless, the trend is that the ITB is triggered mainly by negative magnetic shear during the transient preformed current phase, then maintained by the $\mathbf{E} \times \mathbf{B}$ shear stabilizing effect, for about 2 s during the current flat top.

*Present address: Princeton Plasma Physics Laboratory, P.O. Box 451, Princeton, NJ 08543.

[1] F. M. Levinton *et al.,* Phys. Rev. Lett. **75,** 4417 (1995).
[2] E. J. Strait *et al.,* Phys. Rev. Lett. **75,** 4421 (1995).
[3] S. Ishida *et al.,* Phys. Rev. Lett. **79,** 3917 (1997).
[4] C. Gormezano *et al.,* Phys. Rev. Lett. **50,** 5544 (1983).
[5] M. Hugon *et al.,* Nucl. Fusion **32,** 33 (1992).
[6] G. T. Hoang *et al.,* Nucl. Fusion **34,** 75 (1994).
[7] Equipe Tore Supra, presented by B. Saoutic, in *Plasma Physics and Controlled Nuclear Fusion Research (Proceedings of the 16th International Conference, Montreal, 1996)* (IAEA, Vienna, 1997), Vol. I, p. 141.
[8] M. Greenwald *et al.,* Nucl. Fusion **28,** 2199 (1988).
[9] S. M. Kaye *et al.,* Nucl. Fusion **37,** 1303 (1997).
[10] P. Rebut *et al.,* in *Plasma Physics and Controlled Nuclear Fusion Research (Proceedings of the 12th International Conference, Nice, 1988)* (IAEA, Vienna, 1989), Vol. II, p. 191.
[11] G. T. Hoang *et al.,* Nucl. Fusion **38,** 117 (1998).
[12] L.-G. Eriksson *et al.,* Nucl. Fusion **33,** 1037 (1993).
[13] G. T. Hoang *et al.,* in *Proceedings of the 23rd European Conference on Controlled Fusion and Plasma Physics, Kiev, 1996* (European Physical Society, Geneve, 1996), Vol. 20C, Pt. I, p. 19.
[14] G. Antar *et al.* (to be published).
[15] P. Maget *et al.,* Nucl. Fusion **39,** 949 (1999).
[16] J. W. Connor and R. J. Hastie, Nucl. Fusion **13,** 221 (1973).
[17] P. Platz *et al.* (to be published).
[18] R. Waltz *et al.,* Phys. Plasmas **1,** 2229 (1994).